A Model El Niño–Southern Oscillation*

STEPHEN E. ZEBIAK AND MARK A. CANE

Lamont-Doherty Geological Observatory of Columbia University, Palisades, NY 10964

(Manuscript received 1 December 1986, in final form 23 March 1987)

ABSTRACT

A coupled atmosphere–ocean model is developed and used to study the ENSO (El Niño/Southern Oscillation) phenomenon. With no anomalous external forcing, the coupled model reproduces certain key features of the observed phenomenon, including the recurrence of warm events at irregular intervals with a preference for three to four years. It is shown that the mean sea surface temperature, wind and ocean current fields determine the characteristic spatial structure of ENSO anomalies. The tendency for phase-locking of anomalies is explained in terms of a variation in coupling strength associated with the annual cycle in the mean fields. Sensitivity studies reveal that both the amplitude and the time scale of the oscillation are sensitive to several parameters that affect the strength of the atmosphere–ocean coupling. Stronger coupling implies larger oscillations with a longer time scale. A critical element of the model oscillation is the variability in the equatorial heat content of the upper ocean. Equatorial heat content increases prior to warm events and decreases sharply during the events. A theory for this variability and the associated transitions between non-El Niño and El Niño states is presented. Implications of the model results for the prediction of El Niño events are discussed.

1. Introduction

The collection of atmospheric and oceanic phenomena known as El Niño and the Southern Oscillation (ENSO) have been the subject of intense interest and study over the past several years, especially in the wake of the dramatic episode of 1982/83. Observational studies have identified the global dimensions of the climate variations associated with the Southern Oscillation, and their close association with changes in the surface temperature and current structure of the tropical Pacific Ocean. Many modeling studies have been undertaken, each attempting to reproduce some major feature or features of the observations and thus to identify the set of interactions that can account for this preferred mode of interannual variability in the ocean–atmosphere system. Meteorological studies, using both complex and simple models, point to the importance of tropical Pacific sea surface temperature (SST) anomalies in producing observed atmospheric anomalies during ENSO (e.g., Rowntree, 1972; Wells, 1979; Keshavamurty, 1983; Shukla and Wallace, 1983; Zebiak, 1982, 1986; Gill and Rasmusson, 1983; Webster, 1981; Lau, 1981). Oceanographic studies show that the observed tropical Pacific SST and sea level anomalies during ENSO result primarily from the influence of surface wind stress anomalies (e.g., Busalacchi and O'Brien, 1981; Cane, 1984; Philander and Siegel, 1985). The combined results identify the interactive nature of the phenomenon and show the need for a model that allows for such interaction. Although much of the behavior of each component of the system can be reproduced with existing models by specifying the state of the other, little has been said about the behavior of the coupled system. For example, questions concerning initiation, duration, termination and irregular recurrence of ENSO events remain unanswered.

To date there have been only a few attempts at studying the coupled problem. McWilliams and Gent (1978) and Lau (1981) have examined highly idealized models and demonstrated the possibility of low-frequency variability in the coupled system that is absent in the individual components. McCreary (1983) and McCreary and Anderson (1984) present models with explicit ocean dynamics but highly idealized atmospheres. They also find interannual variability under certain assumptions. Vallis (1986) has shown that the presence of nonlinearities in an otherwise idealized coupled model can lead to *aperiodic* oscillations.

Philander et al. (1984) examine a model with explicit linear dynamics for both the atmosphere and the ocean. They find a coupled instability that leads to the growth of large-scale atmospheric and oceanic anomalies. The development is arguably similar to the growth of anomalies during ENSO, although the linearizations of the model do not permit equilibration and the subsequent decay of anomalies. In a more recent study, Philander (1985) presents a model which, with different assumptions concerning air–sea coupling, simulates the decay phase of ENSO. As pointed out by the author, the two versions of the model are incompatible because of the highly parameterized form of the coupling. Thus

* Contribution Number 4192 of the Lamont-Doherty Geological Observatory of Columbia University.

the two cannot be combined in their present form to describe the full ENSO cycle.

Anderson and McCreary (1985) use a more sophisticated nonlinear ocean model with explicit dynamics and thermodynamics, and they couple it to a linear atmosphere model, attempting to describe the evolution of the total SST and wind fields. They find interannual variability of the coupled system, though the spatial and temporal characteristics of the anomalies differ somewhat from the real system. This may be related to the difference in background states; that is, the model climatology differs considerably from the observed mean state. The nonlinear coupled model of Schopf and Suarez (private communication) produces a somewhat different climatology and correspondingly gives different interannual variability.

Rennick and Haney (1986) and Hirst (1986) analyze in detail linear, free (i.e., unbounded) modes of the coupled system. Again, low-frequency oscillatory modes are found under a number of different assumptions. A major limitation of these studies is the absence of oceanic boundaries. The boundaries are known to affect the oceanic response qualitatively at low frequency.

All of these results indicate that interannual variability can result from interaction between the tropical ocean and atmosphere. However, many specific questions regarding ENSO remain unanswered. For example, why does the system continue to oscillate on interannual time scales, rather than seeking a more uniform annually periodic state? What determines the preferred period of 3–4 years, and what are the probable sources of aperiodicity? What accounts for the characteristic temporal and spatial patterns of ENSO anomalies? Here we attempt to address some of these questions and to build on the earlier studies of ENSO, using a coupled model of the tropical Pacific Ocean and atmosphere. The atmospheric component of the coupled model has been described in Zebiak (1986; hereafter referred to as Z). It was shown to produce equatorial wind and convergence anomalies similar to observations when forced by observed ENSO SST anomalies, despite certain systematic discrepancies in the off-equatorial response. The oceanic component of the model has been described in Zebiak (1984). The model was shown to reproduce key features of the observed SST anomalies during ENSO, when forced using observed tropical wind anomalies. The present coupled model differs from others in its treatment of the thermodynamics in the atmosphere and ocean, especially through the inclusion of a moisture feedback process in the atmosphere and a thermodynamically active (though simplified) surface layer in the ocean.

The remainder of this paper is organized as follows. The model components are reviewed in section 2, and the results from an extended (90 year) coupled run are presented in section 3. Section 4 examines certain model parameter sensitivities. The role of the annual cycle is analyzed in section 5, and in section 6, we present a theory for the ENSO cycle, based on the coupled model results. A summary and concluding remarks follow in section 7.

2. Model description

The model components have been presented in detail previously and will only be summarized here. (The full governing equations are given in the Appendix.) Both components describe perturbations about the mean climatological state, with the climatology specified from observations. The Climate Analysis Center dataset (see Rasmusson and Carpenter, 1982) was used for this purpose.

a. Atmosphere

The dynamics follow Gill (1980), i.e., steady-state, linear shallow-water equations on an equatorial beta plane. Linear dissipation in the form of Rayleigh friction and Newtonian cooling is used. The circulation is forced by a heating anomaly that depends partly on local heating associated with SST anomalies and partly on the low-level moisture convergence (parameterized in terms of the surface wind convergence). Several observational studies (e.g., Cornejo-Garrido and Stone, 1977; Ramage, 1977), as well as GCM calculations, have demonstrated the important contribution of moisture convergence to the overall tropical heat balance.

The convergence feedback is incorporated into the model using an iterative procedure in which the heating at each iteration depends on the convergence field from the previous iteration. The scheme is analyzed in detail in Z. The feedback is nonlinear because the moisture-related heating is operative only when the total wind field is convergent, and this depends not only on the calculated convergence anomaly, but also on the specified *mean* convergence [see Eq. (A3)]. As shown in Z, the important effect of the feedback is to focus the atmospheric response to SST anomalies into or near the regions of mean convergence, in particular, the Intertropical Convergence Zone (ITCZ) and the South Pacific Convergence Zone (SPCZ). Such focusing is conspicuous in the observed wind anomalies during ENSO (see Rasmusson and Carpenter, 1982).

b. Ocean

The model ocean basin is rectangular and extends from 124°E to 80°W and from 29°N to 29°S. The dynamics of the model begin with the linear reduced-gravity model [Eqs. (A4)–(A7)] that has been used successfully in simulating thermocline depth anomalies and surface pressure changes during El Niño events (Busalacchi and O'Brien, 1981; Cane, 1984; Busalacchi and Cane, 1985). Such models produce only depth-averaged baroclinic currents, but the surface current is usually dominated by the frictional (Ekman) com-

ponent. Therefore, a shallow frictional layer of constant depth (50 m) is added to simulate the surface intensification of wind-driven currents in the real ocean. The dynamics of this layer are also kept linear, but only by using Rayleigh friction to stand in for nonlinear influences at the equator [Eqs. (A8)–(A9)]. As is common in reduced-gravity models, the surface layer pressure gradient varies only with the thermocline depth. This assumption neglects the influence of any temperature changes occurring in the surface layer alone (i.e., changes uncorrelated with those below). This influence is usually, but not universally, negligible; hence its neglect cannot be justified rigorously.

Mean surface currents were generated by spinning up the model with monthly mean climatological winds. These currents were then specified in the anomaly calculations.

The thermodynamics describe the evolution of temperature *anomalies* in the model surface layer. The governing equation includes three-dimensional temperature advection by both the specified mean currents and the calculated anomalous currents. The assumed surface heat flux anomaly is proportional to the local SST anomaly, acting always to adjust the temperature field toward its climatological mean state, which is specified from observations.

This parameterization is clearly oversimplified and is probably incorrect in some local regions, but nonetheless it agrees with the general results of observational studies (Ramage and Hori, 1981; Weare, 1983).

Using the above formulations, the thermodynamic equation has the following form (where barred quantities represent mean fields and unbarred quantities represent anomalies):

$$\frac{\partial T}{\partial t} = -\bar{\mathbf{u}}_1 \cdot \nabla T - \mathbf{u}_1 \cdot \nabla(\bar{T}+T) - \{M(\bar{w}_s + w_s) - M(\bar{w}_s)\} \times \bar{T}_z - M(\bar{w}_s + w_s)T_z - \alpha_s T, \quad (1)$$

where $\mathbf{u}_1$ and w_s represent horizontal surface currents and upwelling, respectively, and the function $M(x)$ is defined by

$$M(x) = \begin{cases} 0, & x \leqslant 0 \\ x, & x > 0. \end{cases} \quad (2)$$

This function accounts for the fact that surface temperature is affected by vertical advection only in the presence of upwelling. The anomalous vertical temperature gradient, T_z, is defined by

$$T_z = (T - T_e)/H_1, \quad (3)$$

where H_1 is the surface layer depth, and T_e measures temperature anomalies entrained into the surface layer. The model parameterizes subsurface temperature anomalies in terms of thermocline motions, which can be equated to the model upper-layer thickness variations.

The parameterization arises by assuming a fixed vertical temperature profile for the thermocline structure and simply displacing this profile up and down with the thermocline depth [as determined by the shallow-water dynamics, i.e., Eqs. (A4)–(A6)] This temperature profile is estimated from observations and fit to a simple functional form [Eq. (A13)]. We find that this form crudely approximates observed temperature changes below the mixed layer in the equatorial region as a function of longitude and season. In particular, since the mean thermocline depth is shallow in the east Pacific, the subsurface temperature field is more sensitive to anomalous thermocline displacements there, in accord with observations. We emphasize that this is an empirical relationship. While it appears to account for much of the observed temperature variability below the surface layer, it cannot distinguish between the various processes contributing to that variability in the real ocean.

In Zebiak (1984) it was shown that this ocean model simulates the mean features of the observed SST anomalies when forced by ENSO composite wind anomalies and that the full complexity of (1) is required to achieve this.

c. *Coupling*

The ocean component is forced by surface wind stress anomalies. A standard bulk formula is used to generate stress anomalies from the combination of surface wind anomalies produced by the atmosphere model and the background mean winds. The ocean dynamics time step is 10 days.

The atmosphere model is steady-state and was previously run with specified monthly mean SST anomalies to simulate monthly mean wind anomalies. In the present context, the wind field must be determined at 10-day increments. There are several possible approaches. On one extreme, the model could be used exactly as before, calculating the steady response to the SST anomaly field at each time step. This implicitly assumes that the atmosphere adjusts very rapidly [O(2–3) days] to changes in boundary forcing and cannot be justified. On the other extreme, time dependence could be added explicitly to the model. This would be computationally costly, since a time step of order 2 h would be required for inertial gravity waves. Moreover, it is unnecessary because the important limiting time scale is the longer one associated with the equilibration of the heating field, i.e., the moisture convergence feedback process. We adopt a third alternative: allowing time dependence only in the moisture convergence component of the heating. With this scheme, the change in heating is computed at each time step, and the assumed background convergence is the total convergence at the previous time step, rather than just the mean convergence (as in the steady-state model). Because of the nonlinearity of the heating parameterization, this time-marching procedure allows the development of small-scale anomalies that can persist and become unrelated to subsequent SST anomaly patterns.

We have found that the simplest and most effective way to prevent this is to recalculate the heating periodically using the steady model formulation, based on the current SST anomaly field. (This strategy is similar to the periodic restarts often used with the leapfrog scheme to suppress splitting of the solution.) In the model run to be presented in section 3, the recalculation was done once per month. The result of using a different criterion is discussed in section 4. In addition to the above, a maximum of three feedback iterations is performed at each time step. This affects only the very small-scale features of the response (see Z) and not the larger-scale features that characterize the ENSO signal. The net result is similar to applying spatial smoothing and requires less computation.

To summarize, the calculation of the atmospheric heating has been split into two parts. The portion related directly to SST operates the same as in Z and gives a wind response in equilibrium with the SST field on a time scale of 10 days. The portion of the heating related to internal moisture convergence feedback operates in a time-stepping sense, and so forces a wind field adjustment on a somewhat longer time scale (of order 1 month or more).

3. Results: Standard case

The following is a description of a 90-year run of the coupled model. The run was initiated with an imposed westerly wind anomaly of the form

$$u_a = (2\,\mathrm{m\,s^{-1}}) \exp[-(y/20°)^2] \qquad (4)$$

in the region 145°E to 170°W. The anomaly was held fixed for a period of four months (from December until April of the first year) and then removed. Thereafter there is no external forcing. All parameter values for the model are as specified in the previous uncoupled calculations of Zebiak (1984, 1986) and are listed in the Appendix.

Figure 1 shows a time record of area-averaged SST anomalies for the regions 5°N–5°S, 90°–150°W, and 5°N–5°S, 150°W–160°E, designated as NINO3 and NINO4, respectively. A striking result is the recurrence of warm events, deriving solely from self-interactions of the coupled system. After the first, rather weak warm event in year 0 (which results from the imposed initial condition), the system exhibits quasi-regular oscillations with a favored period of 3–4 years. The oscillations appear at times to be very regular in amplitude and structure, while at other times they are noticeably nonuniform, with variable amplitude and inter-event spacing. Once initiated, however, the development of the major warm episodes is very closely tied to the annual cycle. They tend to peak either in June or around the end of the year and have a total duration of between 14 and 18 months. The larger events exceed 2°C in the east (and 3°C at the eastern boundary). During the mature phase of warm events, the largest SST anomalies occur in the east, with decreasing amplitude toward the west (NINO3 > NINO4). Also, the anomalies tend to peak first in the east and later in the central region.

Figure 2, taken from Rasmusson and Carpenter (1982), shows a comparable time series computed from observations spanning the period 1921–76. Many similar characteristics are evident. For example, the oscillations are irregular but exhibit a strong preference for a 3–4 year period. Major warm events have a duration

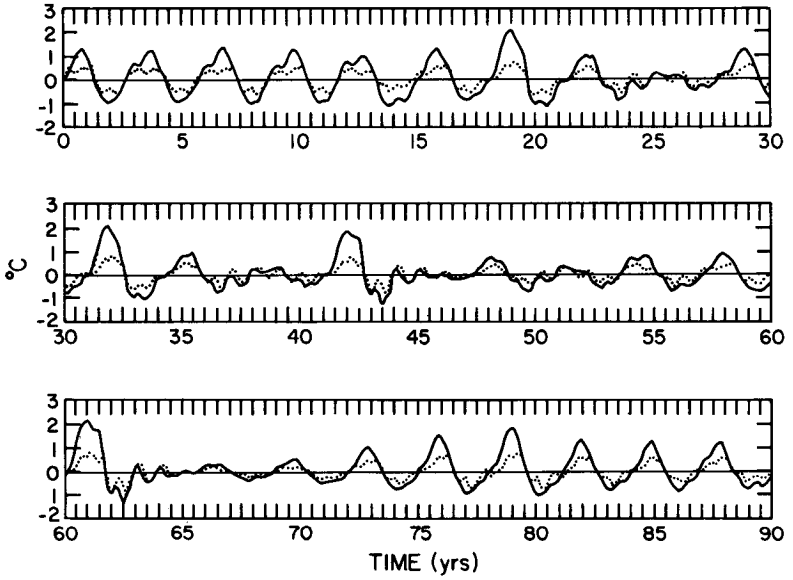

FIG. 1. Area-averaged SST anomalies for the 90-year model simulation. The solid line is NINO3 (5°N–5°S, 90°–150°W), and the dotted line is NINO4 (5°N–5°S, 150°W–160°E).

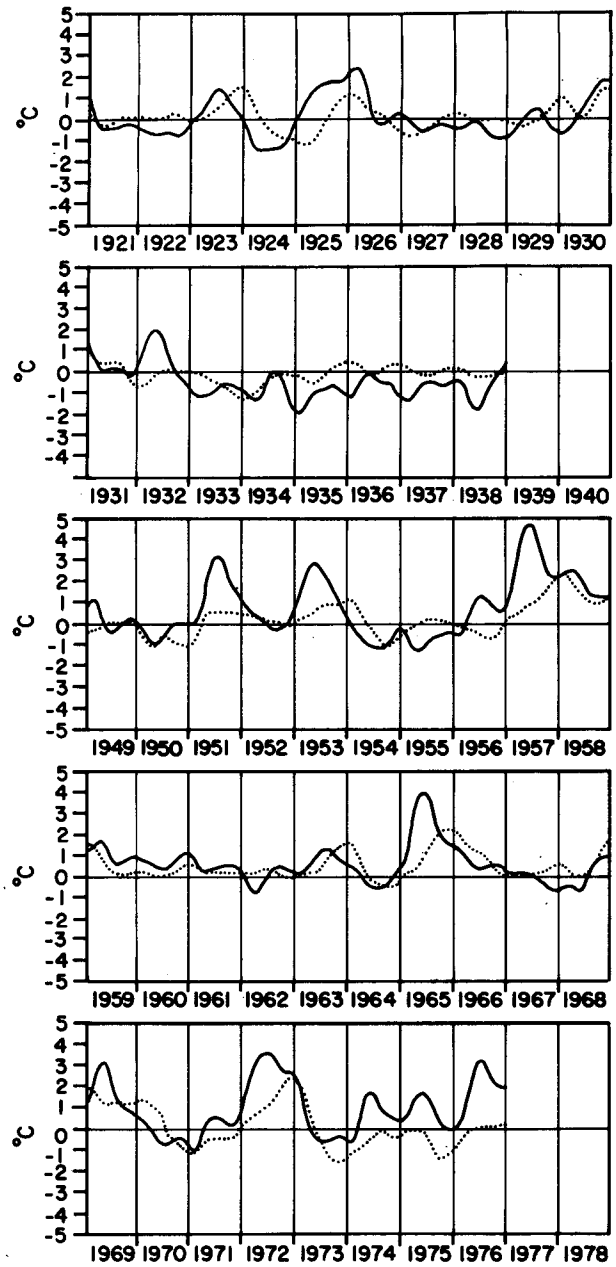

FIG. 2. Observed SST anomalies in the eastern Pacific (solid line) and the central Pacific (dotted line) (after Rasmusson and Carpenter, 1982).

of somewhat more than a year and develop in a systematic fashion, with maximum amplification of central Pacific anomalies in (northern) summer and peaking of anomalies around the end of the year. The largest anomalies occur in the eastern Pacific and typically range between 2° and 4°C for major ENSO events.

A notable difference between the model results and the observations is the lack of an initial coastal warming in the model, such as is often, but not always, observed prior to the major central Pacific warming. The ocean model was unable to reproduce this feature even when forced by composite ENSO winds, so the result is hardly surprising here. The success of the simulation apart from this feature suggests that the details of the temperature field very near the east coast are not fundamental to the evolution of the larger-scale anomalies.

Figure 3 shows a time series of area-averaged wind anomalies for the 90-year simulation. Two indices, representing equatorial zonal wind anomalies in the western Pacific (5°N–5°S, 135°E–180°) and the eastern central Pacific (5°N–5°S, 180°–140°W), are shown. The former is designated TW1 and the latter TW2. The primary temporal characteristics are very similar to those of the temperature indices, although the wind indices exhibit more high-frequency variability. During major warm events, the two indices vary in a similar fashion, indicating a very large scale coherent wind forcing, whereas during periods without major warm events the two indices are often out of phase, indicating smaller scale wind patterns with less net influence on the ocean. As in the atmospheric calculation using prescribed SST anomalies, the western Pacific zonal wind anomalies are weaker than observed and switch from westerly to easterly later than observed.

A more detailed picture of the evolution of SST and wind anomalies during a warm event is given in Figs. 4–11, which trace the development in three-month intervals between the end of year 30 and year 32. The period is characterized by one of the larger warm events of the 90-year simulation (see Fig. 1).

The sequence begins in December of year 30 (Fig. 4), at which time there are no appreciable anomalies in either SST or wind. By March(31)[1] (Fig. 5) a region of warm SST anomaly has developed in the equatorial zone east of 170°W, with a maximum near 130°W. Associated with this are small westerly wind anomalies in the region 130° to 160°W. The warm event is well underway by June(31) (Fig. 6), with SST anomalies exceeding 1°C in the eastern equatorial Pacific and sizeable ($\sim$1 m s^{-1}) westerly wind anomalies in the central Pacific. As indicated above, the warming in the eastern ocean tends to occur uniformly, rather than initially at the coast. Most, but not all, observed events exhibit the earlier coastal anomaly. We believe this discrepancy is due, at least in part, to the lack of adequate resolution of the ocean model near the eastern boundary. This would lead to an underestimation of the response to both local and remote forcing.

The observed tendency for expansion and amplification of both SST and wind anomalies in the fall of an ENSO year also occurs in the model. By September(31) (Fig. 7), warm anomalies extend as far westward as 160°E, and eastern Pacific anomalies exceed 2°C.

[1] Hereafter, the number given in parentheses after a month is the year of the 90-year simulation.

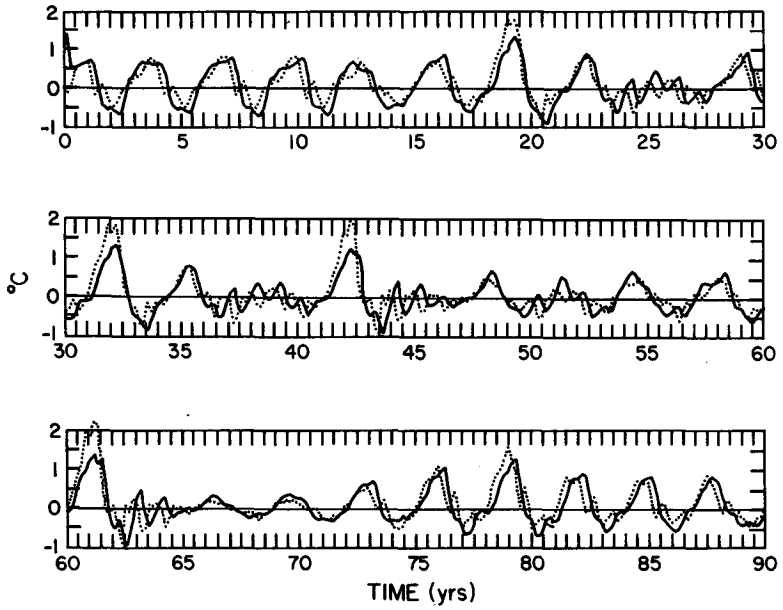

FIG. 3. Area-averaged zonal wind anomalies (m s^{-1}) for the 90-year model simulation. The solid line is TW1 (5°N–5°S, 135E°–180°), and the dotted line is TW2 (5°N–5°S, 180°–140°W).

Large westerly wind anomalies cover the whole equatorial central Pacific, with equatorward flow across the normal position of the ITCZ. The easterly anomalies in the eastern Pacific are not realistic. They also appeared in the uncoupled calculation using observed SST anomalies (see discussion in Z). In agreement with the composites, a region of small negative SST anomaly and easterly wind anomaly has developed in the western Pacific at this time.

The peak temperature anomalies occur in December(31) (Fig. 8), with a maximum at the coast and another one near 140°W. By December the SST anomalies also have expanded meridionally, compared with the preceding patterns. These features are realistic, except that the coastal maximum is exaggerated. This was also the case for the uncoupled ocean model. Both the model and the composites show westerly wind anomalies of about 2 m s^{-1} in the central Pacific at this time. However, observations also show the development of easterly anomalies in the western Pacific. This feature does not develop in the model either at this time or in the immediately ensuing months. The somewhat delayed termination of the model warm event can be traced to this.

By March(32) (Fig. 9), temperature anomalies have begun to decrease, especially at the east coast. A single

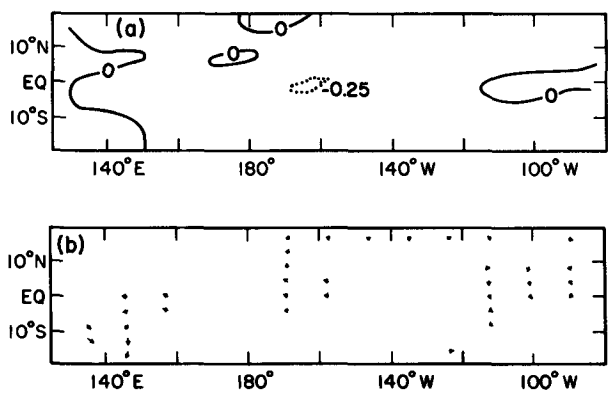

FIG. 4. (a) SST anomalies and (b) wind anomalies in December of year 30 of the model simulation.

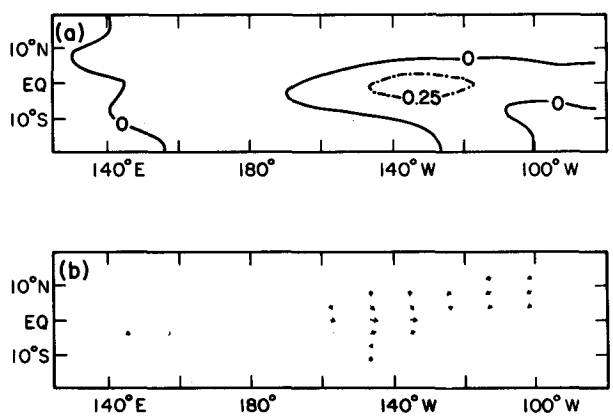

FIG. 5. As in Fig. 4, except for March of year 31.

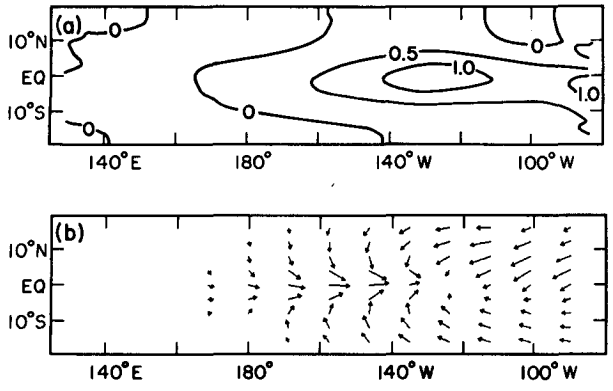

FIG. 6. As in Fig. 4, except for June of year 31.

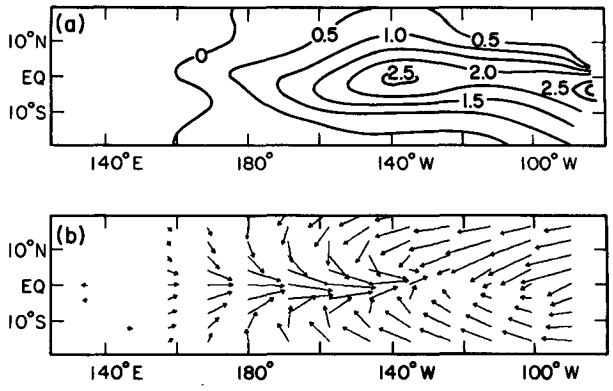

FIG. 8. As in Fig. 4, except for December of year 31.

maximum now exists in the eastern central Pacific. The pattern is quite similar to the composite event for this time, although the amplitude of the warm anomaly is about a factor of two larger than the composite. Very large westerly wind anomalies persist in the central Pacific, with increasing easterly anomalies farther to the east.

In June(32) (Fig. 10), the eastern ocean is still warm, though temperatures are decreasing rapidly. The westerly wind anomalies have decreased and receded westward, and stronger easterlies are evident in the east. By this time, the composites show cold SST anomalies and poleward wind anomalies in the eastern ocean.

During the summer of year 32 a dramatic change occurs in both winds and SST, amounting to a rapid termination of the warm event. By September(32) (Fig. 11), the equatorial eastern and central ocean is cold, and the winds are primarily meridional and directed poleward. The temperature pattern is not unlike that of the composite for this time, which also shows an equatorial tongue of cold anomaly extending across much of the basin.

All of the major warm events in the model evolve in a similar fashion. Some of the smaller amplitude anomalies develop differently and do not conform to the canonical scenario. This may be true in reality as well. Only the large anomalies have been studied intensively, and moreover, the focus has been on the common features of the events rather than their individual characteristics.

An important element of the coupled system oscillation is the oceanic heat exchange in the equatorial region. Figure 12 displays the model thermocline depth anomaly $h(x, t)$ along the equator between years 30 and 45 of the coupled run. This variable may be interpreted as a measure of the heat content of the upper ocean. The major warm episodes (beginning in years 31 and 41) are characterized by anomalously high heat content in the east and low heat content in the west for a period of nearly a year. This occurs approximately in phase with the strong and sustained westerly wind anomalies in the central Pacific (Fig. 13).

Superimposed on the east–west exchanges of heat is a fluctuation in the zonal mean heat content of the equatorial region. The periods preceding major warm events are characterized by above-normal heat content at all longitudes (early in years 31 and 41), and the periods immediately following warm events show a

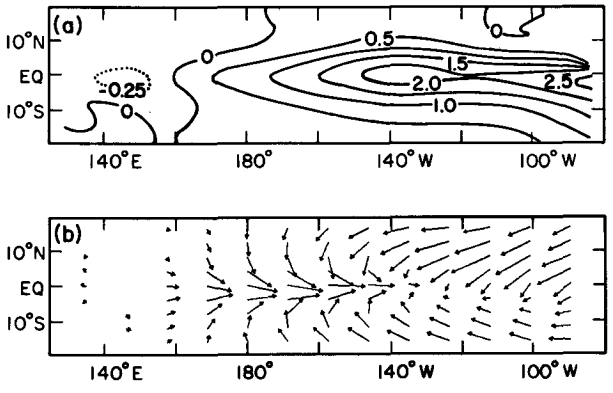

FIG. 7. As in Fig. 4, except for September of year 31.

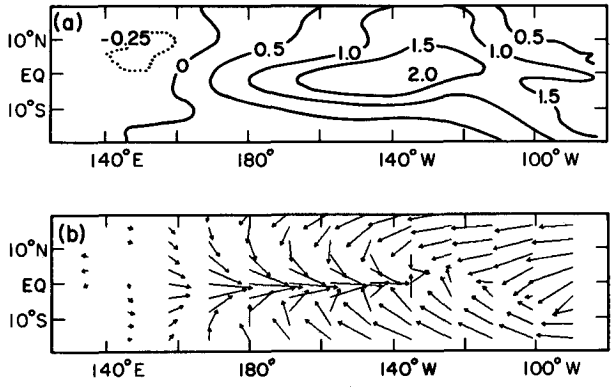

FIG. 9. As in Fig. 4, except for March of year 32.

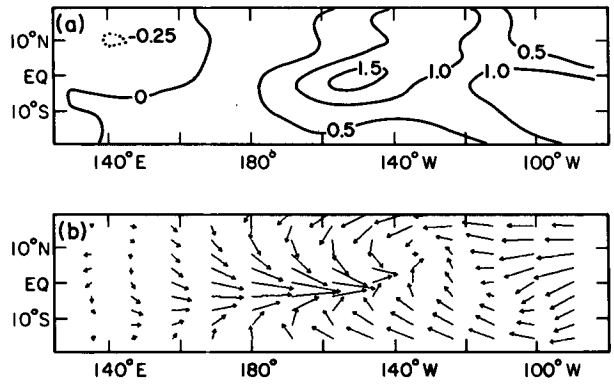

FIG. 10. As in Fig. 4, except for June of year 32.

corresponding deficit of heat content (late in years 32 and 42). It is important to note that the rise in net equatorial heat content precedes the development of equatorial westerlies and positive SST anomalies in the eastern ocean; that is, it precedes the ENSO event. This suggests that such a rise in equatorial heat content may be a precondition for ENSO. We will return to this point in section 6. Also, note that the fluctuations in heat content under consideration here are strictly adiabatic; they arise from variations in the upper-layer thickness induced by wind stress forcing alone.

As seen from the preceding results, the signature of model warm events is a large-scale pattern of equatorial westerly wind anomalies in the central Pacific and equatorial SST anomalies that extend across most of the basin and decrease in amplitude from east to west. This characteristic structure derives from the effects of the mean SST, wind and current fields. The climatological mean state includes easterly trade winds blowing across the eastern and central ocean. The easterly stress induces equatorial upwelling and sets up a sizeable zonal tilt to the thermocline, such that the cold, subthermocline water is far removed from the surface in the west, and very near the surface in the east. Because of the proximity of the main thermocline to the surface,

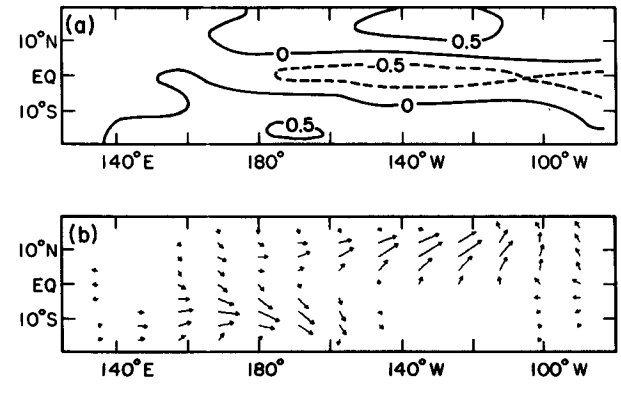

FIG. 11. As in Fig. 4, except for September of year 32.

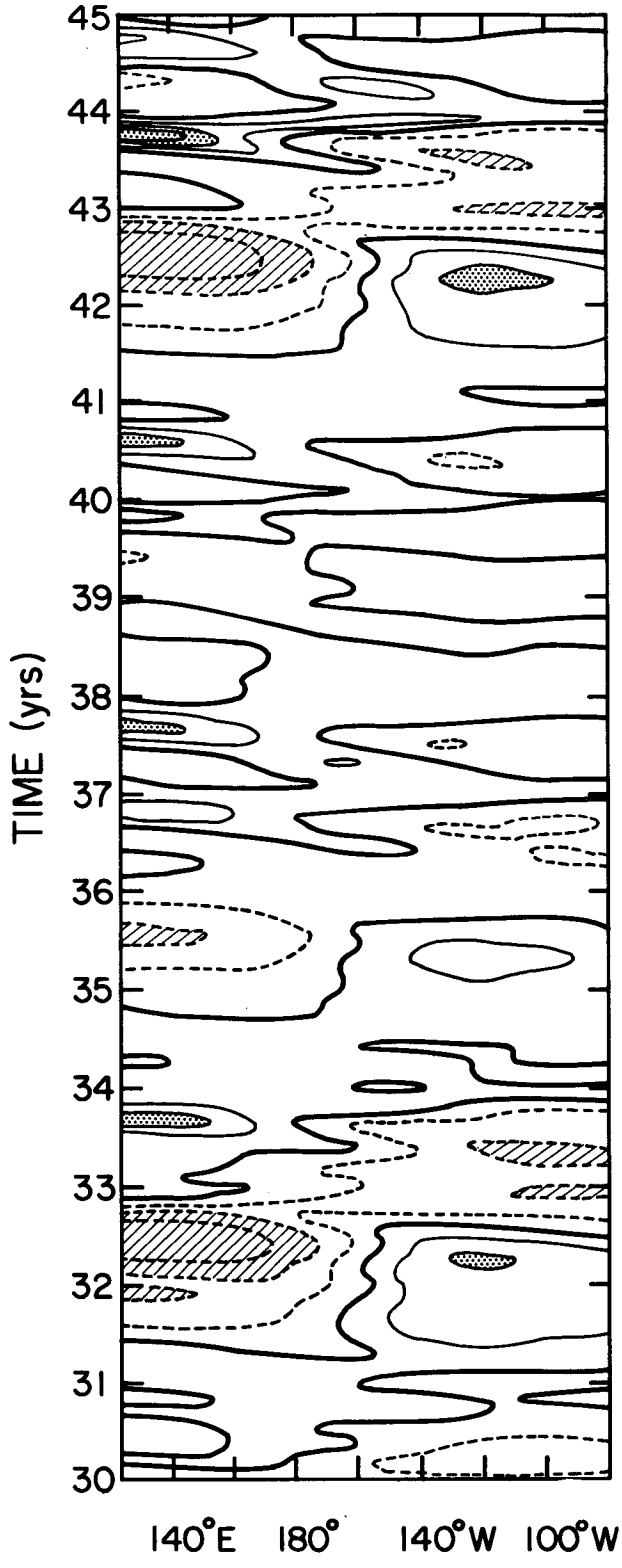

FIG. 12. Model thermocline depth anomaly at the equator between year 30 and year 45 of the 90-year simulation. Positive anomalies are indicated with solid lines, and negative anomalies are indicated with dashed lines. The contour interval is 10 m. Anomalies greater than +20 m are stippled; anomalies greater than −20 m are hatched.

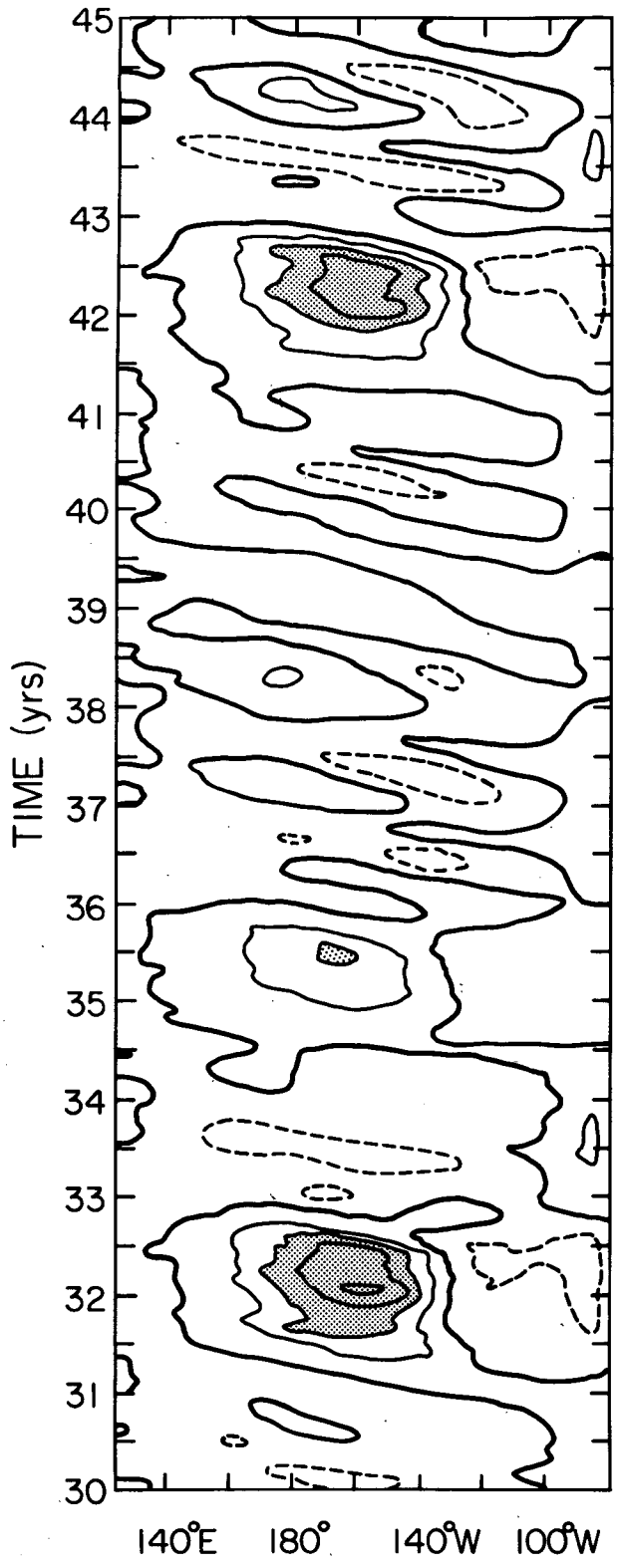

FIG. 13. Equatorial zonal wind stress anomalies between year 30 and year 45 of the model simulation. Positive (westerly) anomalies are indicated with solid lines, and negative (easterly) anomalies are indicated with dashed lines. Large westerly anomalies (≥0.15 dyn/cm^{-2}) are stippled.

a given anomaly in upper-layer depth results in a subsurface temperature anomaly that is largest in the east and smaller toward the west. In the presence of mean upwelling, a similar anomaly pattern is readily established in the surface layer as well. Thus, due to the mean state of the tropical ocean, there is a natural tendency to produce SST anomalies that are largest in the east and decreasing toward the west. In the case of a large-scale positive SST anomaly pattern of this type, the atmospheric response includes equatorial westerly anomalies that span nearly the entire region of SST anomalies (see Z, and references cited there). The influence of the westerly wind anomalies is (a) to deepen the eastern ocean thermocline, (b) to supress equatorial upwelling, and (c) to set up eastward current anomalies, all of which tend to reinforce the temperature anomaly pattern Thus, the feedback between the two media is positive, leading to the sustained growth of large-scale anomalies in their characteristic spatial modes. This is how the model warm events develop. The development is not unlike that found in the linear model of Philander et al. (1984), except for the preferred spatial structure. One aspect of the observations not found in the model is the tendency for gradual eastward migration of atmospheric anomalies during the course of the warm event (Rasmusson and Gill, 1983). We find that this is better captured by the atmosphere component alone when forced with observed SST anomalies. The lack of such a feature in the coupled model is at least partly due to the tendency of the ocean component to understate temperature anomalies in the western Pacific.

Figure 13 shows that the model behavior during inter-event periods differs from that during warm events. The inter-event periods are characterized by easterly anomalies that tend to develop in the eastern ocean and propagate rapidly westward. They are well correlated with similarly propagating anomalies in SST (not shown). There is little evidence of such features in observations. These rather small-scale, coupled anomalies can develop and persist in the model because a portion of the atmospheric heating is related directly to local SST anomalies, regardless of spatial or temporal scales. In the real system, the local response to small-scale, transient features is probably diminished by the effects of moisture and temperature advection in the boundary layer.

At times during the model simulation, westerly anomalies appear in a fashion similar to the onset of a warm event, but the development quickly terminates (Fig. 13, years 38 and 44). The difference between these two situations seems to be the presence of easterly anomalies in the eastern Pacific. In the aborted event cases, easterly anomalies exist in the east at the time the westerly anomalies appear farther west. As the westerlies grow, the easterlies do so as well, and shortly thereafter the development ceases. Preceding warm events, on the other hand, there are no significant easterly anomalies in the east, either before the appearance

of westerly anomalies or during their growth. The development of easterly anomalies can in turn be traced to the time of year the would be warm event is getting established. In each case of a terminated event, the initial growth occurs in the early part of the year (January–March). The substantial warm events, on the other hand, start later (April–June). This suggests that the annual cycle exerts considerable influence over the development of ENSO events. Section 5 addresses the role of the annual cycle in greater detail.

It was found that the processes contributing to SST variability in the coupled model are essentially the same as was found with the ocean model alone when forced with observed winds. In the coastal upwelling zone, the mean upwelling advection is dominant, with smaller contributions from the remaining terms (all acting in the same sense). In the eastern equatorial Pacific, zonal advection and anomalous upwelling also contribute importantly to the development, especially during the mature phase of the warm events. For the western and central equatorial region, the net effect of vertical advection is negligible, and zonal advection is dominant.

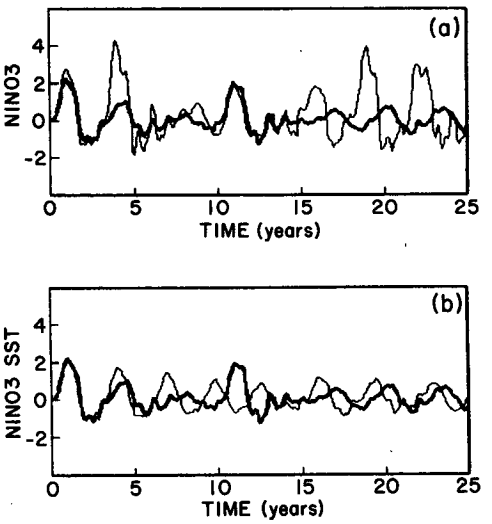

FIG. 14. (a) NINO3 for the 25-year period starting at year 31 of the standard (90-year) run (heavy line) and corresponding curve for a test run starting from the same initial conditions with the atmospheric heating parameter α increased by 10% (thin line). (b) Similar comparison between the standard run and a test run with the atmospheric convergence feedback parameter β increased by 7%.

4. Model sensitivities

In this section we examine the sensitivity of the model to some of its parameterizations. Since a complete treatment of model sensitivities cannot feasibly be presented here, we will discuss only a selected set of experiments that illustrate the principal variations in model behavior we have found. A more extensive treatment is provided in Zebiak (1984). Each of the sensitivity experiments is a 25-year run, starting from the same initial conditions. The initial conditions are taken from the beginning of year 31 of the 90-year run (the wind and SST anomalies at this time are shown in Fig. 4). It should be noted, however, that the results are *not* sensitive to the initial conditions. Characteristic changes in model behavior, where present, appear consistently for widely varying initial states. For brevity, the results are shown only in terms of the NINO3 SST anomaly index. We are thus focusing on the temporal characteristics and amplitudes of large-scale anomalies.

a. Atmospheric parameterizations

Two experiments were done with variations in the atmospheric heating parameterization. In the first experiment, the coefficient of the heating term proportional to SST anomalies [i.e., α in Eq. (A3a)] was increased by 10%. The NINO3 index from this run and from the standard run are shown together in Fig. 14a. Despite the modest increase in heating strength, there is a large increase in the characteristic amplitude of anomalies. Other properties of the earlier solution, however, are preserved; i.e., there are still irregular oscillations with a preferred time scale of 3–4 years. This suggests that the sensitivity of the oscillation amplitude is much greater than that of the oscillation time scale. Other experiments with both increased and decreased values of α confirm this. The results also illustrate the degree to which the atmosphere–ocean coupling can amplify anomalies that might occur in either the atmosphere or the ocean alone. For prescribed SST anomalies, a 10% increase in α could produce, at most, a 20% increase in wind stress anomalies. In the coupled model, however, it produces roughly a 100% increase.

In the second experiment, the coefficient of the component of heating proportional to low-level moisture convergence [i.e., β in Eq. (A3b)] was increased by 7%. The results (Fig. 14b) show that the general characteristics of the solution are unchanged. This seems somewhat surprising, given the fact that the net latent heating depends sensitively on β (as shown in Z). However, the sensitivity to β is scale-selective, with predominantly the smaller scales being affected as β increases. Apparently, the net impact on the larger-scale structure is minimal.

b. Oceanic parameterizations

The experiments of this type include the following:

(i) a decrease of 30% in surface layer thermal dissipation (the decay time is increased from 125 days to 160 days);

(ii) an increase of 20% in the drag coefficient (used in the bulk formula that relates model winds to wind stress);

(iii) an increase of 30% in all mean current speeds;

(iv) a decrease of 13% in the oceanic equivalent depth (from 86 to 75 cm);

(v) an increase of 16% in the oceanic equivalent depth (from 86 to 100 cm);

(vi) a decrease of 30% in subsurface layer momentum dissipation (the decay time is increased from 30 months to 42 months).

The results of the six cases are shown in Figs. 15a–f, respectively. Judging from cases (i)–(iv), it is clear that the sensitivites to thermal dissipation, drag coefficient, mean currents and equivalent depth are all large. In each of these cases both the amplitude and the time scale of the oscillations increase. What is remarkable is the degree to which these different parameter changes (and others) produce the same result. Cases (i)–(iii) are virtually indistinguishable in their characteristics, and case (iv) differs only in being more nearly periodic. The parameter changes in these experiments all act to increase SST anomalies for fixed atmospheric anomalies. Reduced thermal dissipation clearly allows larger SST anomalies. A larger drag coefficient produces greater wind-stress forcing for the ocean, resulting in larger anomalies of all types. Stronger mean upwelling yields larger SST anomalies in response to thermocline displacements. Finally, a smaller equivalent depth (for a fixed wind stress) produces larger thermocline variations and thus larger subsurface temperature anomalies. In the upwelling regions this again translates into larger SST anomalies. In the coupled model, all of these effects induce an atmospheric response that further reinforces them; i.e., they increase the strength of the atmosphere–ocean coupling. Thus, the results indicate that an increase in coupling strength, regardless of how it is achieved, results in oscillations with larger amplitude and period. Experiment (v) offers one example of a parameter change in the opposite sense, that is, one which amounts to decreasing the coupling strength. The result in this case is smaller oscillations with a shorter period. Other cases of decreased coupling strength (not shown) are similar.

Experiment (vi) illustrates a case of low sensitivity. As seen from Fig. 15f, a sizeable decrease in background ocean dissipation produces no change in the characteristics of the sólution. In other experiments with much larger dissipation (decay times of order 1 year), the amplitude of the oscillations is noticeably reduced, but the preferred period remains the same.

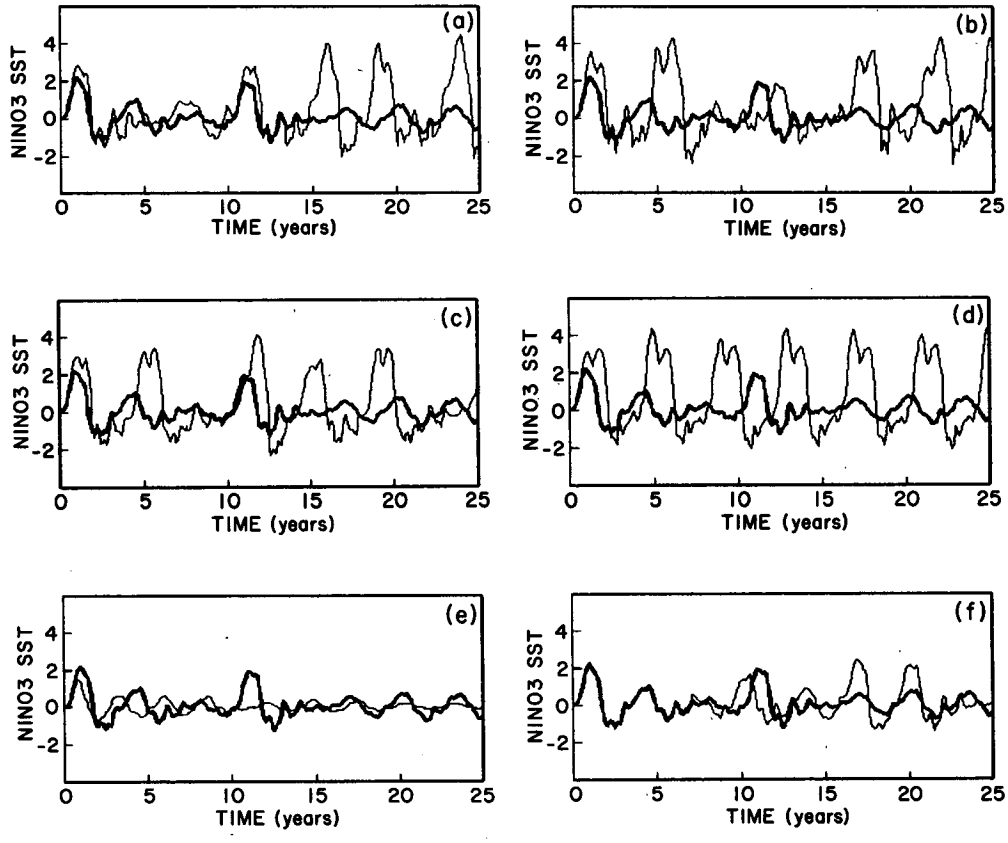

FIG. 15. Comparison of standard run (heavy line in each case) and test runs (thin line) with (a) oceanic surface-layer thermal dissipation decreased by 30%, (b) drag coefficient increased by 20%, (c) mean currents increased by 30%, (d) oceanic equivalent depth decreased by 13%, (e) oceanic equivalent depth increased by 16%, and (f) subsurface layer momentum dissipation decreased by 30%.

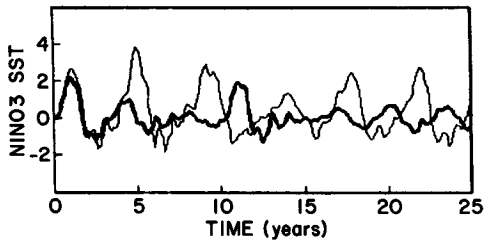

FIG. 16. Comparison of standard run (heavy line) and a test run (thin line) with alternate coupling procedure (see text).

c. Coupling procedure

The coupling procedure described in section 2 involves recalculating the total atmospheric anomalies once a month and computing incremental changes otherwise. The recalculation prevents the eventual growth of unphysical small-scale features in the model winds. We have also examined a somewhat different procedure: recalculation of the wind anomalies only at those times when the temperature anomalies (as measured by NINO3) are very small. This procedure gives a less frequent recalculation (once per month is more than is needed), but since the recalculation is now linked to the ENSO cycle itself, it avoids introducing a separate time scale into the system. The results are shown in Fig. 16. The characteristic amplitude of oscillations increases, and the favored period increases from 3 years to 4 years. Along the lines of the previous discussion, this alternate procedure appears to increase the coupling strength somewhat. In either case, however, the characteristics of the variability lie within realistic limits.

5. Influence of the annual cycle

Both real and model warm events are clearly tied to the annual cycle, tending to amplify sharply during the (northern) summer, reach peak amplitude around the end of the year, and diminish during the following year. In order to examine the annual cycle influence in the model, a set of experiments was done in which the annual cycle was turned off at various points during the evolution of a warm event. For each experiment, initial conditions were taken from January of year 31 of the standard run (a warm event year), and the annual cycle was turned off at a given subsequent month by holding the mean fields fixed from then on. Four cases are shown, corresponding to suppressing the annual cycle in April(0), August(0), December(0), and July(1), where year 0 represents the warm event year.

Figure 17a shows the evolution of NINO3 from the standard run and from the April(0) experiment. With the background fields held in their April configurations, the growth of the warm event is retarded considerably. The amplitude increases more slowly, reaches a maximum several months later, and then decreases sharply.

When the annual cycle is suppressed in August(0), the result is very different (Fig. 17b). The amplitude continues to rise sharply for many months into year 1, peaking later and at a larger value than with the annual cycle included. The subsequent decline is similar to that during the summer period for the annual cycle case.

In the standard run, the warm event has reached maximum amplitude and is subsiding by December(0). The result of maintaining December conditions from then on is shown in Fig. 17c. There is an immediate and steady decline into the middle of year 1, as opposed to a hesitation in the decline during the early part of year 1 if the annual cycle is maintained. The later development of negative anomalies, on the other hand, is suppressed relative to the annual cycle case.

If July conditions are maintained from July(+1) onward (Fig. 17d), then compared to the standard case, the growth of negative anomalies continues longer and leads to larger anomalies during year(+2). This is analogous to the situation for the growth of positive anomalies in the August(0) experiment.

The results demonstrate that the annual cycle influences the development of anomalies significantly. The August(0) and July(1) experiments indicate that the (northern) summer period is most favorable for rapid growth of both positive and negative anomalies. The remainder of the cases indicate that the spring period is least favorable for anomaly growth and that the fall and winter periods are intermediate. In terms of the discussion in section 4, we can interpret the results as

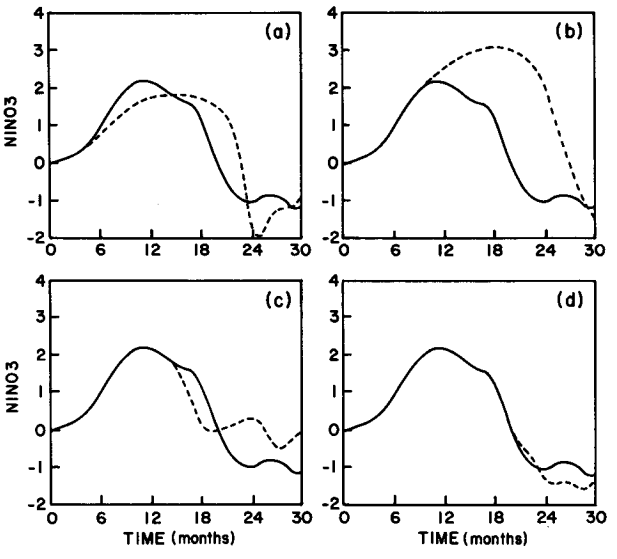

FIG. 17. Comparison of NINO3 for the 30-month period starting from January of year 31 of the standard run (heavy solid lines) and (a) test run with April conditions maintained after month 4, (b) test run with August conditions maintained after month 8, (c) test run with December conditions maintained after month 12, and (d) test run with July conditions maintained after month 19. Test runs are shown by the dashed lines.

an indication that the effective coupling strength is modulated by the seasonal variations in mean fields. This interpretation also accounts for the manner in which ENSO anomalies are phase-locked to the annual cycle in the full model. Typically, small anomalies that are present in the spring of an ENSO year amplify rapidly during the summer and fall, reaching large amplitude. During the winter period, the coupling strength begins to decrease significantly and becomes insufficient to maintain the large anomalies against the mechanisms of dissipation (the most significant of which is the thermal damping of the oceanic surface layer), and thus the anomalies begin to decrease. After a hesitation during the spring, an increase in coupling strength during the following summer hastens the demise of the warm event and the growth of negative anomalies.

An examination of the seasonal variations in the mean fields can explain the influence on coupling strength. In the spring season (February–April), the mean equatorial tradewinds are weak (Horel, 1982), as are the associated equatorial upwelling and eastern Pacific SST gradients. All of these act to diminish the growth of anomalies. A given wind anomaly produces a relatively small stress anomaly because the mean wind speed is small. A given subsurface temperature anomaly is less readily transferred to the surface because the upwelling is weak. A given current anomaly is less effective in generating temperature anomalies because the mean temperature gradients are weak. On the other hand, during summer and fall the mean winds, mean upwelling and mean SST gradients are all large, and this period is favorable for anomaly growth. The winter season is intermediate between these two extremes.

Despite the fact that spring is the season of minimum growth rate, it is noteworthy that all the major warm events first appear during this season. This is the time of maximum SST in the eastern Pacific and the time when the ITCZ briefly extends southward to the equator. With mean convergence, the atmospheric feedback mechanism is operative, and there can be considerable local response to SST anomalies. For this reason the spring may be a particularly favorable time for coupled anomalies to become organized. This idea has been put forward previously by Philander (1985).

The results suggest that, even without the annual cycle, the tendency for interannual oscillation persists. The April(0) and August(0) experiments, for example, eventually give a termination of the warm event and subsequent development of negative anomalies, just as in the case with the annual cycle included (although at a later time). Another experiment, illustrated in Fig. 18, examines this issue further. In this experiment, the annual cycle was suppressed in July(0), and the calculation carried on for 25 years. The solution settles into a periodic oscillation with period 47 months. Extended runs using mean conditions from other months (not shown) give somewhat different periods and different amplitudes. It is clear that, although the annual cycle strongly affects the evolution of anomalies (and in particular, the evolution of warm events), it is not essential to the system's tendency for interannual oscillation. Results to date suggest to us that the annual cycle contributes to the aperiodicity of the full model, though we have at present done insufficient calculations to say with confidence that the annual cycle is required to give aperiodicity within the realistic range of model parameters.

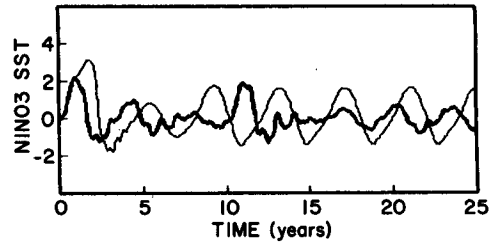

FIG. 18. Comparison of standard run (heavy line) and test run (thin line) with July conditions maintained after July of year 0.

6. Elements of the model oscillation

One of the most robust characteristics of the model simulations is the tendency for oscillation on interannual time scales. The oscillatory behavior persists over a considerable range of parameter values and with or without the influence of the annual cycle. Since there is no anomalous external forcing, this must result from some internal characteristics of the coupled system. However, the previous calculations have not clearly identified the causes of the oscillation or what sets its time scale. They have shown only that the time scale (and amplitude) of the oscillation is affected by a subtle composite of many different physical parameters. During the El Niño, or warm event phase of the oscillation, the development clearly depends on a positive feedback between large-scale atmospheric and oceanic anomalies. The feedback allows sustained anomalies in both the atmosphere and the ocean that would not persist in either medium alone. The same argument could be made with regard to anomalies of the opposite sign during non–El Niño periods. But what causes the transitions between these two states? As discussed in the previous section, the annual cycle can stop the growth of anomalies at a particular time if its effects are included in the model. In its absence, there are yet other mechanisms of equilibration. For example, the ocean thermodynamics can produce surface temperatures no greater than the warmest temperature of the mean state, as temperature variations result solely from advective processes, and the heat flux anomalies always act in a dissipative manner. These effects insure that anomalies do not grow to arbitrarily large amplitude but do not explain why the system oscillates, as opposed to settling into a nonzero equilibrium state (or an an-

nually periodic state with nonzero mean). Some other factor or factors must be responsible for this.

In section 3 we showed that the integrated heat content along the equator varies with a phase that is different from that of the larger east–west fluctuations that characterize warm events (see Fig. 12). The integrated heat content tends to be high prior to the development of a warm event and is low in the aftermath of an event. We describe here some experiments that demonstrate the importance of this effect.

The upper ocean heat content is measured by the model upper layer depth, which approximates the thermocline depth in the real ocean. This variable affects the surface layer thermodynamics only through the parameterized subsurface temperature [Eq. (A13)]. In the following experiments the subsurface temperature was made more or less sensitive to changes in the area-averaged heat content anomaly for the entire equatorial band between 5°N and 5°S. This region encompasses the equatorial upwelling zone, where subsurface anomalies can be expected to affect surface temperature. In the first experiment, subsurface temperature anomalies were made completely insensitive to changes in the average heat content of the region. This amounts to replacing the variable h in (A13) with the expression $h - h^*$, where h^* is the average of h over the region of interest. Note that this does not alter the temperature variations associated with the zonal slope of the equatorial thermocline; i.e., it does not suppress the dominant ENSO signal. It does, however, suppress the temperature signal associated with any uniform raising or lowering of the thermocline in this region. Initial conditions were again taken from the beginning of year 31 of the standard run. Figure 19a shows the evolution of NINO3 over 25 years in the experimental run, together with the same index from the standard run. The result of suppressing the effects of changes in integrated heat content is dramatic: the system no longer oscillates, but rather moves immediately toward a new climatology with only annual variability. The new climatology represents an El Niño–like state, with relatively warm eastern ocean temperatures and weak equatorial trades. If the experiment is started at a time when h^* is negative rather than positive (as in this case), the solution moves correspondingly toward a climatology with colder SST and stronger trades. In either case, there is no interannual oscillation; the ENSO cycle does not survive.

In a second experiment, exactly half of the actual fluctuation in h^* was allowed to influence temperature; i.e., the variable h in (A13) was replaced by the expression $h - 0.5h^*$. The result is shown in Fig. 19b. There is now an interannual oscillation with amplitude similar to the original run, but with a characteristic period of 5–6 years, nearly twice as long as before.

Finally, the temperature effect associated with h^* was enhanced by a factor of three [the variable h in (A13) was replaced by the expression $h + 2h^*$]. As

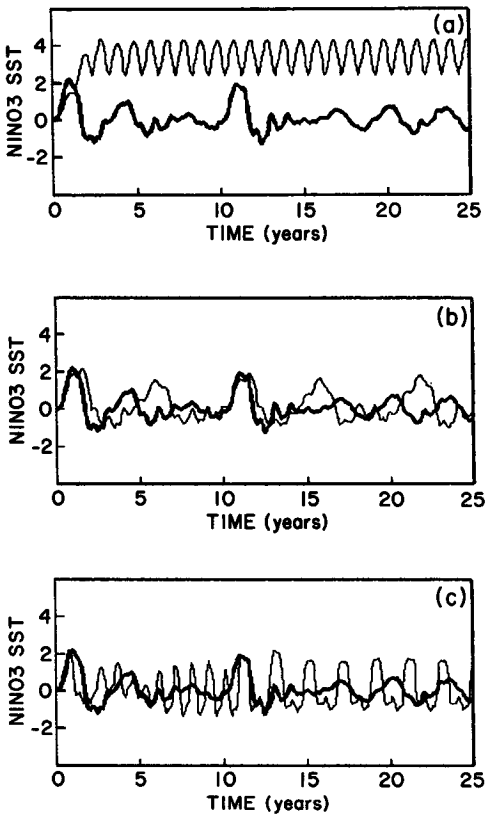

FIG. 19. Comparison of standard run (heavy line) and test run (thin line) with (a) effects of variations in equatorial heat content suppressed (see text), (b) effects of variations in equatorial heat content reduced by 50%, and (c) effects of variations in equatorial heat content increased by 200%.

shown in Fig. 19c, the result is an oscillation that, again, is similar to before in amplitude, but now exhibits a much shorter period of 1–2 years.

The results show empirically that the oscillatory character of the coupled system depends on the effect of variations in net equatorial heat content. Without this effect, there is no oscillation. If the effect is partially suppressed, the transitions between cold and warm states are retarded. If the effect is enhanced, the transitions are hastened. Fluctuations in net heat content similar to those of the coupled model are produced by the linear ocean dynamics alone, in response to basin-scale low-frequency periodic wind forcing (Cane and Sarachik, 1981). In this forced case, the same phase lead of h^* occurs; that is, h^* is positive prior to the westerly wind phase of the cycle and negative following this phase. In addition, the response is such that the changes in thermocline depth in the eastern part of the basin lead the changes in the winds by a fraction of the oscillation period. This property holds for all periods significantly greater than the Kelvin wave crossing period, (i.e., for periods of order a year or more), with the precise degree of phase shift depending on frequency (among other factors).

In the coupled model, the winds are not specified, but rather are calculated from the SST field. The SST field, however, is affected strongly by thermocline motions in the eastern part of the basin (where there is vigorous upwelling and the mean position of the thermocline is close to the surface), and thus the winds are strongly coupled to thermocline motions there. Moreover, the coupling is such that changes in wind stress tend to lag changes in thermocline depth. This is because it takes finite time for upwelling effects to create surface temperature anomalies from subsurface anomalies, and for the mean surface currents to spread the anomalies over a region large enough to influence the atmosphere significantly. The phase lag between wind stress and thermocline is in precisely the same sense as is required by the equatorial ocean dynamics for low-frequency oscillatory modes. We propose that it is because of this possible matching of phase relations that oscillations of the coupled system are possible.

If there were a simple, linear relationship between thermocline depth and wind stress, the theory would predict perfectly regular oscillations of the coupled system (though in general they would be exponentially increasing or decreasing in amplitude). Of course, this is not the case in the full model. Many processes come into play in relating thermocline motions to surface wind stress, and others act somewhat independently, e.g., zonal temperature advection in the oceanic surface layer and moisture convergence effects in the atmosphere. The thermocline influence itself is a nonlinear function in the full model. Furthermore, all of these processes are subject to seasonal variability associated with the annual cycle. Apart from providing negative feedbacks at large amplitude which limit the growth of anomalies, these effects tend to obscure otherwise uniform phase relations that would exist in a simpler, linear system. It is because of this that the nonlinear oscillations of the full model can exhibit variability in amplitude and period. Despite this, there is clearly a preference for 3–4 year periods. According to the present theory, this reflects a characteristic, if somewhat variable, time delay between dynamical changes in the eastern ocean and associated large-scale fluctuations in equatorial wind stress.

7. Summary and conclusions

We have presented a coupled model that is used to simulate and study ENSO. The coupled model calculates perturbations about a (monthly) climatological mean state that is specified from observations. Without anomalous external forcing, the coupled model produces recurring warm events that are irregular in both amplitude and spacing, but favor a 3–4 year period, as observed. The events develop systematically, with the largest growth occurring during the (northern) summer and fall and termination during the following spring and summer. The signature of model warm events includes equatorial westerly wind anomalies in the central Pacific and large SST anomalies in the eastern Pacific. These features are in general agreement with observations. In the model, the characteristic spatial patterns result from the configuration of the mean wind, current and temperature fields. The phase-locking occurs because the seasonal variations in these mean fields effectively modulate the coupling strength between atmospheric and oceanic anomalies.

Despite the model's successes, it is limited in its ability to simulate the real system. A detailed comparison with observations shows discrepancies in both the atmospheric and oceanic simulations. We expect that the model can rather easily be improved in some respects and that better simulations will be possible with more sophisticated models.

Experiments with the model show that both the amplitude and the time scale of the cycle are sensitive to certain parameters. All parameter changes which amounted to increasing (decreasing) the strength of the atmosphere–ocean coupling tended to produce larger (smaller) amplitudes and longer (shorter) periods. In no case, however, was interannual variability eliminated. This is true even in experiments with the annual cycle removed. The mechanism of low-frequency oscillation in the model is highly robust.

A critical element of the model oscillation is the variation in net heat content of the near-equatorial ocean. There is a buildup in heat content prior to the onset of a warm episode and a rapid decrease in heat content during the course of the event. Though this signal is small relative to the east–west fluctuations that characterize the extremes of the cycle, it is not unimportant. In experiments where the effects of this fluctuation were artificially suppressed, the ENSO cycle was eliminated. Similar fluctuations should be evident in the real ocean if the model is correctly simulating the ENSO cycle.

The variations in equatorial heat content are characteristic of bounded equatorial ocean dynamics for low-frequency oscillatory forcing, and a concomitant of these fluctuations is a systematic phase lag between wind stress and thermocline motions in the eastern part of the basin. We have suggested that, within a certain parameter range, the physics of the coupled model allows such a phase relation between these fields, and that this is why interannual oscillations occur in the *coupled* system. More work will be required to substantiate and possibly refine this theory. We have pointed to three elements that we believe are essential to the interannual oscillations observed in the coupled model. First, there is a positive feedback between large-scale atmospheric and oceanic anomalies. In other words, the background state of the coupled system is unstable to El Niño–like perturbations. Second, there are nonlinear mechanisms of equilibration that prevent the anomalies from growing to arbitrarily large amplitude. Dominant among these are the limits imposed

by the mean thermal structure of the ocean (in particular, the structure of the thermocline). These effects are important in determining the characteristic amplitude range of anomalies. Finally, due to the nature of the atmosphere–ocean coupling, there is a systematic, though somewhat variable, time delay between dynamical changes in the eastern ocean and associated large-scale fluctuations in equatorial wind stress. Due to the unique characteristics of equatorial ocean dynamics, this gives rise to a continuing succession of transitions between non–El Niño and El Niño states on interannual time scales. The transitions are a result of the linear shallow-water dynamics and not other, less familiar aspects of the model. The presence of nonlinear processes in the model additionally allows the possibility of aperiodicity.

If the model is correctly simulating the real ENSO cycle, then the results have a number of implications. First, a necessary precondition for the onset of a warm episode is above-normal equatorial heat content. This is not a sufficient condition, so it cannot take the place of a forecast model. However, it can identify favorable periods and can exclude others. Second, all the mechanisms essential to the ENSO cycle are contained within the tropical Pacific region alone. This does not preclude the possibility of teleconnections to other regions. Finally, we need not appeal to random forcing of unknown origin in order to account for the aperiodicity of ENSO; it can result from strictly deterministic processes. All of these bear favorably on the prospects for prediction of El Niño. Along these lines, we have found that the same model as presented here has skill in forecasting ENSO at lead times of 1–2 years (Cane et al., 1986). This, we believe, adds further weight to the argument that ENSO is largely controlled by deterministic processes in the tropical Pacific atmosphere–ocean system.

Acknowledgments. We are deeply appreciative of the support for this work provided by Adrian Gill. Our thanks to the many colleagues, notably including the reviewers of an earlier version, whose comments and criticisms have contributed to an improved manuscript. Thanks to Karen Streech and Naomi Katz for invaluable help in preparing the manuscript. This work has been supported by grants NAGW-916 from NASA and NA-84-AA-D-00031 of the U.S. TOGA Project Office of NOAA.

APPENDIX

Governing Equations of the Coupled Model

The governing equations for the atmosphere (at iteration n) are as follows (see Zebiak, 1986):

$$+\epsilon u_a^n - \beta_0 y v_a^n = -(p^n/\rho_0)_x \quad \text{(A1)}$$

$$\epsilon v_a^n + \beta_0 y u_a^n = -(p^n/\rho_0)_y \quad \text{(A2)}$$

$$\epsilon(p^n/\rho_0) + c_a^2[(u_a^n)_x + (v_a^n)_y] = -\dot{Q}_s - \dot{Q}_1{}^{n-1} \quad \text{(A3)}$$

$$\dot{Q}_s = (\alpha T)\exp[\bar{T} - 30°\text{C})/16.7°\text{C}] \quad \text{(A3a)}$$

$$\dot{Q}_1{}^n = \beta[M(\bar{c} + c^n) - M(\bar{c})], \quad \text{(A3b)}$$

where

$$M(x) = \begin{cases} 0, & x \leq 0 \\ x, & x > 0. \end{cases} \quad \text{(A3c)}$$

In (A3a), $\bar{T}(x, y, t)$ is the prescribed monthly mean SST, and T is the anomalous SST. In (A3b), $\bar{c}(x, y, t)$ is the prescribed monthly mean surface wind convergence, and c^n is the anomalous convergence at iteration n, defined by

$$c^n \equiv -(u_a^n)_x - (v_a^n)_y. \quad \text{(A3d)}$$

The governing equations for the ocean (see Zebiak, 1984) are

$$u_t - \beta_0 y v = -g' h_x + \tau^{(x)}/\rho H - ru \quad \text{(A4)}$$

$$\beta_0 y u = -g' h_y + \tau^{(y)}/\rho H - rv \quad \text{(A5)}$$

$$h_t + H(u_x + v_y) = -rh, \quad \text{(A6)}$$

where

$$\mathbf{u} = H^{-1}(H_1 \mathbf{u}_1 + H_2 \mathbf{u}_2). \quad \text{(A7)}$$

The subscripts 1 and 2 refer to the surface layer and underlying layer, respectively.

The equations governing the shear between layers 1 and 2 are

$$r_s u_s - \beta_0 y v_s = \tau^{(x)}/\rho H_1 \quad \text{(A8)}$$

$$r_s v_s + \beta_0 y u_s = \tau^{(y)}/\rho H_1, \quad \text{(A9)}$$

where $\mathbf{u}_s \equiv \mathbf{u}_1 - \mathbf{u}_2$.

Equations (A4)–(A9) allow the surface current $\mathbf{u}_1$ to be determined. From this, the entrainment velocity is calculated:

$$w_s = H_1[(u_1)_x + (v_1)_y]. \quad \text{(A10)}$$

The temperature equation for the surface layer is, then,

$$\frac{\partial T}{\partial t} = -\mathbf{u}_1 \cdot \nabla(\bar{T} + T) - \bar{\mathbf{u}}_1 \cdot \nabla T - \{M(\bar{w}_s + w_s) - M(\bar{w})\} \times \bar{T}_z - M(\bar{w}_s + w_s)\frac{T - T_e}{H_1} - \alpha_s T, \quad \text{(A11)}$$

where $\bar{\mathbf{u}}_1(x, y, t)$ and $\bar{w}_s(x, y, t)$ are the mean horizontal currents and upwelling, respectively, $\bar{T}(x, y, t)$ is the prescribed mean SST, and $\bar{T}_z(x)$ is the prescribed mean vertical temperature gradient. The entrainment temperature anomaly, T_e, is defined by

$$T_e = \gamma T_{\text{sub}} + (1 - \gamma)T. \quad \text{(A12)}$$

T_{sub} has the form

$$T_{\text{sub}} = \begin{cases} T_1\{\tanh[b_1(\bar{h} + h)] - \tanh(b_1 \bar{h})\}, & h > 0 \\ T_2\{\tanh[b_2(\bar{h} - h)] - \tanh(b_2 \bar{h})\}, & h < 0, \end{cases} \quad \text{(A13)}$$

where $\bar{h}(x)$ is the prescribed mean upper layer depth.

Parameter values used for the coupled simulation are as follows:

$$\epsilon = (2\ \text{days})^{-1}, \quad c_a = 60\ \text{m s}^{-1}, \quad \alpha = 0.031\ \text{m}^2\ \text{s}^{-3}/^\circ\text{C},$$
$$\beta = 1.6 \times 10^4\ \text{m}^2\ \text{s}^{-2},$$
$$r = (2.5\ \text{years})^{-1},$$
$$c \equiv (g'H)^{1/2} = 2.9\ \text{m s}^{-1}, \quad H = 150\ \text{m},$$
$$H_1 = 50\ \text{m},$$
$$r_s = (2\ \text{days})^{-1}, \quad \alpha_s = (125\ \text{days})^{-1},$$
$$\gamma = 0.75, \quad T_1 = 28^\circ\text{C}, \quad T_2 = -40^\circ\text{C},$$
$$b_1 = (80\ \text{m})^{-1}, \quad b_2 = (33\ \text{m})^{-1}.$$

REFERENCES

Anderson, D. L. T., and J. P. McCreary, 1985: Slowly propagating disturbances in a coupled ocean–atmosphere model. *J. Phys. Atmos. Sci.*, **42,** 615–629.

Busalacchi, A., and J. J. O'Brien, 1981: Interannual variability of the equatorial Pacific in the 1960's. *J. Geophys. Res.*, **86,** 10 901–10 907.

——, and M. A. Cane, 1985: Hindcasts of sea level variations during 1982/3 El Niño. *J. Phys. Oceanogr.*, **15,** 213–221.

Cane, M. A., 1984: Modeling sea level during El Niño. *J. Phys. Oceanogr.*, **14,** 1864–1874.

——, and E. S. Sarachik, 1981: The response of a linear baroclinic equatorial ocean to periodic forcing. *J. Mar. Res.*, **39,** 651–693.

——, S. E. Zebiak, and S. C. Dolan, 1986: Experimental forecasts of El Niño. *Nature,* **321,** 827–832.

Cornejo-Garrido, A. G., and P. H. Stone, 1977: On the heat balance of the Walker circulation. *J. Atmos. Sci.*, **34,** 1155–1162.

Gill, A. E., 1980: Some simple solutions for heat-induced tropical circulation. *Quart. J. Roy. Met. Soc.*, **106,** 447–462.

——, and E. Rasmusson, 1983: The 1982–83 climate anomaly in the equatorial Pacific. *Nature,* **306,** 229–234.

Hirst, A. C., 1986: Unstable and damped equatorial modes in simple coupled ocean–atmosphere models. *J. Atmos. Sci.*, **43,** 606–630.

Horel, J. D., 1982: The annual cycles in the tropical Pacific atmosphere and ocean. *Mon. Wea. Rev.*, **110,** 1863–1878.

Keshavamurty, R. N., 1983: Southern Oscillation: Further studies with a GFDL general circulation model. *Mon. Wea. Rev.*, **111,** 1988–1997.

Lau, K., 1981: Oscillations in a simple equatoral climate system. *J. Atmos. Sci.*, **38,** 248–261.

McCreary, J. P., 1983: A model of tropical ocean–atmosphere interaction. *Mon. Wea. Rev.*, **111,** 370–387.

——, and D. L. T. Anderson, 1984: A simple model of El Niño and the Southern Oscillation. *Mon. Wea. Rev.*, **112,** 934–946.

McWilliams, J. C., and P. R. Gent, 1978: A coupled air–sea model for the tropical Pacific. *J. Atmos. Sci.*, **35,** 962–989.

Philander, S. G. H., 1985: El Niño and La Nina. *J. Atmos. Sci.*, **42,** 2652–2662.

——, and A. D. Siegel, 1985: Simulation of El Niño of 1982–1983. *Proc. 16th Int. Liege Colloq. on Ocean Hydrodynamics.* J. Nihoul, Ed., Elsevier Oceanography Series, Amsterdam, 767 pp.

——, T. Yamagata and R. C. Pacanowski, 1984: Unstable air–sea interactions in the tropics. *J. Atmos. Sci.*, **41,** 604–613.

Ramage, C. S., 1977: Sea surface temperature and local weather. *Mon. Wea. Rev.*, **105,** 540–544.

——, and A. M. Hori, 1981: Meteorological aspects of El Niño. *Mon. Wea. Rev.*, **109,** 1827–1835.

Rasmusson, E. M., and T. H. Carpenter, 1982: Variations in tropical sea surface temperature and surface wind fields associated with the Southern Oscillation/El Niño. *Mon. Wea. Rev.*, **110,** 354–384.

Rennick, M. A., and R. L. Haney, 1986: Stable and unstable air–sea interactions in the equatorial region. *J. Atmos. Sci.*, **43,** 2937–2943.

Rowntree, P. R., 1972: The influence of tropical east Pacific Ocean temperatures on the atmosphere. *Quart. J. Roy. Meteor. Soc.*, **98,** 290–321.

Shukla, J., and J. M. Wallace, 1983: Numerical simulation of the atmospheric response to equatorial Pacific sea surface temperature anomalies. *J. Atmos. Sci.*, **40,** 1613–1630.

Vallis, G. K., 1986: El Niño: A chaotic dynamical system? *Science,* **232,** 243–245.

Weare, B. C., 1983: Interannual variation in net heating at the surface of the tropical Pacific Ocean. *J. Phys. Oceanogr.*, **13,** 873–885.

Webster, P. J., 1981: Mechanisms determining the atmospheric response to sea surface temperature anomalies. *J. Atmos. Sci.*, **38,** 554–571.

Wells, N. C., 1979: The effect of a tropical sea surface temperature anomaly in a coupled ocean–atmosphere model. *J. Geophys. Res.*, **84,** 4985–4997.

Zebiak, S. E., 1982: A simple atmospheric model of relevance to El Niño. *J. Atmos. Sci.*, **39,** 2017–2027.

——, 1984: Tropical atmosphere–ocean interaction and the El Niño/Southern Oscillation phenomenon. Ph.D. thesis, M.I.T., 261 pp.

——, 1986: Atmospheric convergence feedback in a simple model for El Niño. *Mon. Wea. Rev.*, **114,** 1263–1271.